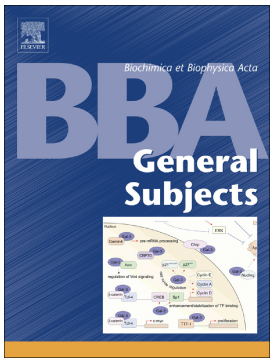

Study of the Cys-his bridge electron transfer pathway in a copper-containing nitrite Reductase by site-directed mutagenesis, spectroscopic, and computational methods

Julio C. Cristaldi, María C. Gómez, Pablo J. González, Felix M. Ferroni, Sergio Dalosto, Alberto C. Rizzi, María G. Rivas, Carlos D. Brondino

PII: S0304-4165(17)30340-9
DOI: doi:10.1016/j.bbagen.2017.10.011
Reference: BBAGEN 28965

To appear in:

Received date: 10 June 2017
Revised date: 6 September 2017
Accepted date: 12 October 2017

Please cite this article as: Julio C. Cristaldi, María C. Gómez, Pablo J. González, Felix M. Ferroni, Sergio Dalosto, Alberto C. Rizzi, María G. Rivas, Carlos D. Brondino , Study of the Cys-his bridge electron transfer pathway in a copper-containing nitrite Reductase by site-directed mutagenesis, spectroscopic, and computational methods. The address for the corresponding author was captured as affiliation for all authors. Please check if appropriate. Bbagen(2017), doi:10.1016/j.bbagen.2017.10.011

Study of the Cys-His Bridge Electron Transfer Pathway in a Copper-containing Nitrite Reductase by Site-directed Mutagenesis, Spectroscopic, and Computational Methods

Julio C. Cristaldi,[a] María C. Gómez,[a] Pablo J. González,[a] Felix M. Ferroni,[a] Sergio Dalosto,[b] Alberto C. Rizzi,[a] María G. Rivas,[a] Carlos D. Brondino [a,*]

[a] Departamento de Física, Facultad de Bioquímica y Ciencias Biológicas, Universidad Nacional del Litoral/CONICET, S3000ZAA Santa Fe, Argentina

[b] Instituto de Física del Litoral, CONICET-UNL, Güemes 3450, S3000ZAA Santa Fe, Argentina

*To whom correspondence should be addressed. E-mail: brondino@fbcb.unl.edu.ar, Fax: + 54-32-4575221

www.fbcb.unl.edu.ar/dfbioq

ABSTRACT

The Cys-His bridge as electron transfer conduit in the enzymatic catalysis of nitrite to nitric oxide by nitrite reductase from *Sinorhizobium meliloti* 2011 (*Sm*Nir) was evaluated by site-directed mutagenesis, steady state kinetic studies, UV-vis and EPR spectroscopic measurements as well as computational calculations. The kinetic, structural and spectroscopic properties of the His171Asp (H171D) and Cys172Asp (C172D) *Sm*Nir variants were compared with the wild type enzyme. Molecular properties of H171D and C172D indicate that these point mutations have not visible effects on the quaternary structure of *Sm*Nir. Both variants are catalytically incompetent using the physiological electron donor pseudoazurin, though C172D presents catalytic activity with the artificial electron donor methyl viologen (k_{cat}= 3.9(4) s^{-1}) lower than that of wt *Sm*Nir (k_{cat}= 240(50) s^{-1}). QM/MM calculations indicate that the lack of activity of H171D may be ascribed to the $N^{\delta 1}H\ldots O{=}C$ hydrogen bond that partially shortcuts the T1-T2 bridging Cys-His covalent pathway. The role of the $N^{\delta 1}H\ldots O{=}C$ hydrogen bond in the pH-dependent catalytic activity of wt *Sm*Nir is also analyzed by monitoring the T1 and T2 oxidation states at the end of the catalytic reaction of wt *Sm*Nir at pH 6 and 10 by UV-vis and EPR spectroscopies. These data provide insight into how changes in Cys-His bridge interrupts the electron transfer between T1 and T2 and how the pH-dependent catalytic activity of the enzyme are related to pH-dependent structural modifications of the T1-T2 bridging chemical pathway.

ARTICLE INFO

Keywords: nitrite reductase, copper, denitrification, *Sinorhizobium meliloti* 2011, enzyme mechanism, electron transfer pathway

Abbreviations: wt *Sm*Nir, wild type nitrite reductase from *Sinorhizobium meliloti* 2011; *Sm*Paz, pseudoazurin from *Sinorhizobium meliloti* 2011; *Rs*, *Rhodobacter sphae*roides 2.4.3,; *Ax, Alcaligenes xylosoxidans*; *Af, Alcaligenes faecalis* S6; MV, methyl viologen; QM/MM, quantum mechanics/molecular mechanics; C172D, a variant form of *Sm*Nir where the Cys172 ligand at the T1 copper center was mutated to aspartic acid; H171D, a variant form of *Sm*Nir where the His 171 ligand at the T2 copper center was mutated to aspartic acid

1. Introduction

Green and blue copper-containing nitrite reductase enzymes (hereafter Nir) catalyze the second step of the denitrification process through the one-electron reduction of NO_2^- to NO ($E^{o'}$ = 370 mV) [1, 2]. In the denitrifying bacterium *Sinorhizobium meliloti* 2011 (*Sm*) this reaction is catalyzed by a green Nir (*Sm*Nir) coded by the structural gene *nirK* [3]. *Sm*Nir, like most green and blue Nir enzymes reported so far [4-9], presents homotrimeric structure with two copper atoms per monomer ~ 12 Å apart, one of type 1 (T1, also blue copper) and the other of type 2 (T2, also normal copper) [10]. T1 and T2 are the electron transfer and the catalytic centers, respectively. The T1 copper ion is tetracoordinated with three strong ligands, two N atoms from histidine imidazoles and a cysteine thiolate group, and a weaker methionine thioether group, in both blue and green Nirs [6, 11]. T2 consists of a four coordinate copper site bound to a labile water molecule and three N atoms from histidine imidazoles in a distorted tetrahedral geometry. The two copper sites are connected by two main chemical pathways; the shorter one, the Cys-His bridge, is thought to transport the electron for nitrite reduction (Figure 1); the longer pathway, which has been called the substrate-sensing loop, is thought to work as a relay to trigger the T1→T2 electron flow through the Cys-His bridge when nitrite is bound to T2 [11-15]. This sensing loop contains an aspartic acid residue that forms a hydrogen bond with the T2 labile water molecule in the resting enzyme state and with the nitrite-T2 complex which was proposed to be essential in catalysis (Figure 1) [16, 17]. The proposed reaction mechanism for Nirs implies a two-proton coupled redox reaction in which nitrite, after binding T2 site having displaced the copper-bound water molecule, is converted to NO by one electron delivered by an external physiological electron donor [12, 14, 18-20]. The physiological electron donor of

*Sm*Nir was identified to be a pseudoazurin (*Sm*Paz) containing only a type 1 copper center [21].

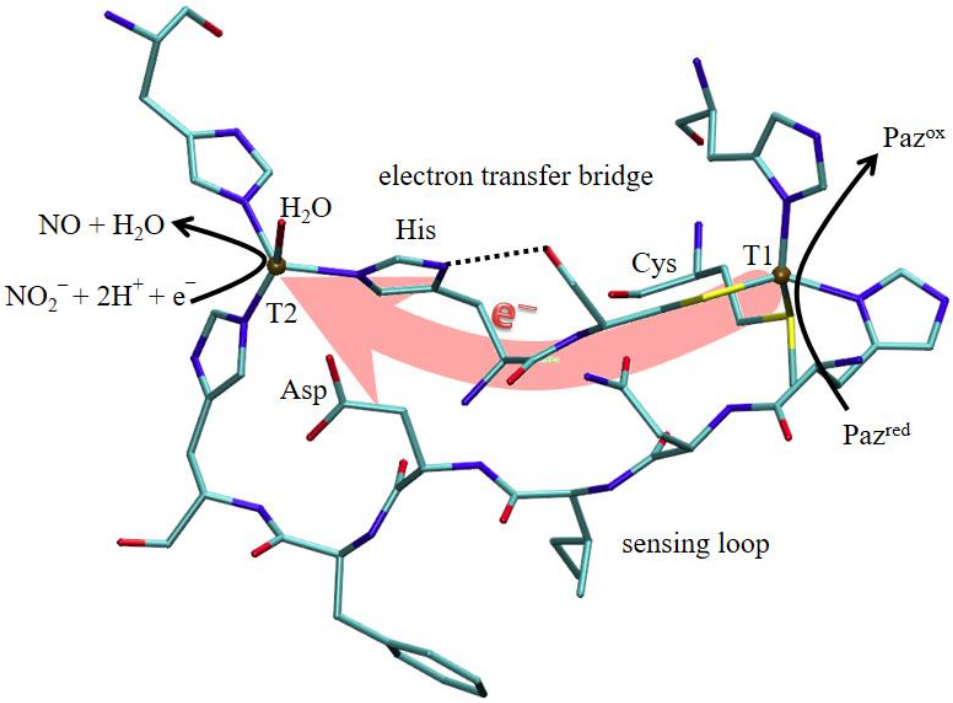

Fig. 1. T1 and T2 copper centers of Nir together with a scheme of the nitrite reduction mechanism. The coordination around the metal centers and the chemical pathways linking both copper centers are shown. The function proposed for each pathway is indicated on the figure. The arrow indicates the electron flow direction through the electron transfer pathway (PDB 1SNR)

Catalytic activity of Nir is maximal at pH ~ 5-6 and drops rapidly at higher pH, which is accompanied with a decrease in T1-T2 electron transfer rate [10, 22-24]. On the basis of X-ray structural studies of Nir from *Rhodobacter sphaeroides* 2.4.3, it was concluded that the tetrahedral geometry distortion of T2 site increases at higher pH [23]. This distortion would lower the T2 reduction potential by ~ 80 mV, which, together with some pH-dependent disorder of a non-coordinated His residue, would preclude an efficient T1→T2 electron

transfer at high pH. These studies also showed that though the T2 site is distorted at pH ~ 8, the metal center retains the capability of binding nitrite, suggesting that the lack of activity at high pH is not associated with substrate binding. Furthermore, the reduction potentials measured for most as-purified Nirs are against a favorable T1→T2 electron transfer reaction, which led to hypothesize that they are modulated upon interaction with nitrite and the physiological donor to favor electron transfer [21, 25-27]. This means that a decrease in potential should cautiously be taken as the possible cause of catalytic activity loss at high pH and that other factors such as the pH-dependent topological characteristics of the Cys-His bridge should also be taken into consideration.

Site directed mutagenesis studies complemented with other techniques such as X-ray crystallography, UV-vis and EPR spectroscopies, kinetic assays, and cyclic voltammetry have been used to analyze the relevance of conserved amino acid residues coordinated and non-coordinated to both copper centers involved in the catalytic mechanism of Nir [5, 17, 28-37]. Some of these studies have been oriented to mutate the amino acid residues involved in the Cys-His chemical bridge. Mutation of the T1 cysteine ligand to alanine in blue *Alcaligenes xylosoxidans* (*Ax*) Nir yielded a protein form having T2 but lacking T1 with no catalytic activity using both physiological and artificial electron donors [29]. Mutation of the T2 histidine ligand to lysine in green *Alcaligenes faecalis* S6 (*Af*) Nir and to valine in blue *Ax*Nir resulted in protein forms containing both T1 and T2 centers, but also completely inactive using both physiological and artificial electron donors [5, 28]. X-ray crystal structure of the protein variant with valine showed a T2 copper coordinated to two His residues only. Although no crystal structure has been reported for the protein variant with lysine, both the long side chain of this amino acid and the positive charge of the ε-amino group at physiological pH suggest that this residue cannot coordinate the T2

copper. To the best of our knowledge, histidine and cysteine protein variants with amino acid residues having a potential coordination ability to copper have not been reported yet. These results altogether indicate that an intact Cys-His bridge is essential for catalysis, but whether the lack of activity of these protein variants was due to either a modified electron transfer chain or to a T2 unable to bind nitrite has not been clarified yet. The Cys-His bridge as electron transfer conduit was also investigated by theoretical calculations [38], which postulated that there are two potential T1→T2 electron transfer subpathways that can selectively be activated depending on the geometric and electronic structure of the T1 Cu site. Whereas in blue Nirs (π-type T1), electron transfer occurs through a pure covalent pathway that involves the protein backbone and the Cys and His side chains (Fig. 1), green Nirs (σ-type T1) perform a more efficient electron transfer through a hydrogen bond-mediated pathway involving the His-$N^{\delta1}$ and the Cys O-carbonyl atoms that partially shortcuts the T1-T2 bridging covalent link (Fig. 1), although no experimental evidence have been reported supporting these calculations. Hereafter this hydrogen bond involved in the electron transfer pathway will be identified as the $N^{\delta1}H\ldots O{=}C$ hydrogen bond.

We report here steady state kinetic studies, UV-vis and EPR spectroscopic measurements, and computational calculations performed on wild type (wt) *Sm*Nir and the protein variants His171Asp (H171D) and Cys172Asp (C172D) obtained by site directed mutagenesis. These mutant proteins are used to explore the effect of modifying the T1-T2 electron transfer chain on catalysis. The role of the $N^{\delta1}H\ldots O{=}C$ hydrogen bond in the pH-dependent catalytic activity of wt *Sm*Nir is also analyzed.

2. Material and methods

2.1. Site-directed mutagenesis

Site-directed mutagenesis of *Sm*Nir was performed by PCR using the p22SK vector as template [10] and H171D-F/H171D-R or C172D-F/C172D-R primers (see Table 1). The PCR mixture contained 8 ng of DNA, 1 μM of each primer, 1.25 units of Long PCR Enzyme Mix (Thermo Scientific), 2.5 μL of PCR reaction buffer (Thermo Scientific), 0.2 mM dNTPs (Genbiotech) in a total volume of 25 μL. The PCR reaction was performed on a Boeco TC-PRO thermocycler using the following program: 3 min at 94 °C followed by 10 cycles of 20 s at 94 °C, 30 s at 57 °C, 7 min at 68 °C, and 20 cycles of 20 s at 94 °C, 30 s at 57 °C, 7 min + 2 s/cycle at 68 °C, and final elongation at 68 °C for 10 min. After amplification procedure, 1 μL of *Dpn* I restriction enzyme (Promega) was added to the constructs and maintained at 37°C for 1 h to eliminate parental methylated and hemimethylated templates. Competent *E. coli* DH5α cells were transformed with digested mixtures. The resulting plasmids encoded the *Sm*Nir variants H171D and C172D. The DNA sequences of both variants were verified by using the Sanger method [39].

Table 1

Primers used to mutate H171 and C172 residues

Primer	Sense	Sequence	Variant
H171D- F	forward	5'-CTTCGTCTACGACTGCGCA- 3'	H171D
H171D- R	reverse	5'-TGCGCAGTCGTAGACGAAG- 3'	
C172D- F	forward	5'- GTCTACCACGACGCACCTC- 3'	C172D
C172D- R	reverse	5'- GAGGTGCGTCGTGGTAGAC- 3'	

2.2. Protein heterologous production and purification

E. coli BL21 (DE3) cells were transformed with p22SK, p22SK_H171D and p22SK_C172D vectors. Each transformed strain was grown aerobically in Lysogeny Broth

containing 100 µg/mL ampicillin at 200 rpm and 37 ºC. Once A_{600} reached 0.6, the culture medium was supplemented with 0.6 mM $CuSO_4 \times 5H_2O$ and the protein expression was induced for 3 h with 0.2 mM Isopropyl-β-D-thiogalactopyranoside (IPTG) at 30 ºC for cells transformed with p22SK and p22SK_H171D, and 0.05 mM IPTG at room temperature for cells transformed with p22SK_C172D.

Cells were then harvested by centrifugation at 5000 × g for 15 min, resuspended in 10 mM Tris-HCl buffer pH 7.0 and disrupted by sonication. The soluble extract was recovered by centrifugation at 12000 × g for 30 min and dialyzed overnight against 10 mM Tris-HCl buffer pH 8.0. The soluble extract containing the C172D variant was subjected to salting out using ammonium sulfate, which was added to the crude extract to a final concentration of 20 % (w/v) with gentle stirring and incubated for 30 min at 4ºC. Soluble protein was collected by centrifugation at 10000 × g for 30 min and dialyzed overnight against 10 mM Tris-HCl buffer pH 8.0.

Extracts were loaded onto a DE52 matrix equilibrated with 10 mM Tris-HCl (pH 8.0 for the variants or 7.0 for wt *Sm*Nir). Wild type *Sm*Nir and H171D were visualized as intense green and gray bands, respectively, whereas C172D was not visually detected. The column was washed with two volumes of equilibration buffer to remove unbound proteins. Then, an ionic strength gradient was performed using five column volumes with NaCl from 0 to 600 mM in 10 mM Tris-HCl buffer. Pure protein fractions were pooled and dialyzed against 10 mM Tris-HCl buffer pH 7.0, concentrated to approximately 18 mg mL^{-1} on an Amicon Ultra 30 K NMWL device, and stored at -80 °C until use. Purity was evaluated by SDS-PAGE.

*Sm*Paz was produced and purified as described previously [21].

2.3. Protein quantification, molecular mass determination, and copper content

Protein concentration was determined using the Lowry method with bovine serum albumin as standard [40].

Protein copper content was determined by Atomic Absorption Spectrometry (Perkin Elmer PinAAcle 900T).

Molecular masses of as-isolated proteins were estimated by gel filtration chromatography (Superdex 200 HR 10/30 column, GE Healthcare) connected to a FPLC device (Akta Basic, GE Healthcare). The column was equilibrated with 50 mM sodium phosphate buffer pH 7.0 plus 150 mM NaCl and calibrated with ferritin (440 kDa), aldolase (158 kDa), conalbumin (75 kDa), carbonic anhydrase (30 kDa), and ribonuclease A (13.7 kDa). Isocratic elution was performed at a flow rate of 0.4 mL min^{-1} with detection at 280 nm. The molecular mass of the subunits was estimated by SDS-PAGE according to the method of Laemmli [41]. Samples were loaded onto a 15% denaturing polyacrylamide gel after treatment with sample buffer for 5 min at 100 °C. Mid-range molecular weight protein standards from Genbiotech were used (Figure S1).

2.4. Activity assays

Activity screening was performed with a continuous method monitoring how dithionite-reduced *Sm*Paz is oxidized by *Sm*Nir when nitrite is added, as described elsewhere [21]. Kinetic assays using methyl viologen (MV) as electron donor were performed using a discontinuous method adapted from a protocol described previously [42, 43]. Solutions containing variable concentrations of sodium nitrite (0-4 mM range) and reduced methyl viologen (1.4 mM plus 100 mM sodium dithionite) were mixed to a final volume of 200 µL. All solutions were prepared in a buffer containing MES, CAPS, and Tris-HCl pH 6 (30

mM each). The kinetic reaction was started by adding 50 µL of 250 nM protein and incubated for 2.5 min at 25 °C. To stop the reaction, 25 µL of each mixture was added to the buffer solution (final volume 250 µL) and immediately vigorously stirred. The solution was reacted with 250 µL of sulfanilamide (1 % in 3 M HCl) and 250 µL of N-(1-naphtyl)ethylendiamine (10 % in buffer) for 10 min, after which a pink color was developed. Absorbance was recorded at 540 nm. The consumed nitrite was determined by comparing the absorbance against a reaction blank without *Sm*Nir.

Kinetic studies were also carried out by cyclic voltammetry as previously reported but using a 3 mm diameter pyrolytic graphite disk working electrode [21]. Measurements were performed on a Teq_4 potentiostat/galvanostat (NanoTeq) and data analyzed using the Teq_4 software package from NanoTeq. Voltammetry results obtained with these modifications did not differ from those previously obtained with a gold disk electrode.

2.5. Spectroscopic methods

Absorption spectra were recorded at room temperature on a Shimadzu UV-1800 UV-vis spectrophotometer.

X-band EPR measurements were performed on a Bruker EMX Plus spectrometer equipped with a universal high sensitivity cavity (HSW10819 model) using a Bruker nitrogen continuous-flow cryostat. Spectra were acquired under non-saturating conditions. Experimental: microwave frequency, 9.45 GHz; modulation field, 100 kHz; modulation amplitude, 2 G; microwave power, 2 mW; temperature, 100 K. EPR spectra were simulated with the EasySpin toolbox based on MATLAB® [44].

Samples for EPR spectroscopy were concentrated to ~200 µM monomeric protein by using an Amicon device. Degassed solutions of sodium ascorbate and sodium dithionite

were withdrawn with gastight syringe from the vessels containing the respective solutions and loaded into argon-flushed EPR tubes containing protein samples (~ 200 µL) followed by gentle mixing. The EPR tubes were frozen with liquid nitrogen and kept under these conditions until use.

2.6. Computational Methods

Since the X-ray structure of *Sm*Nir and their variants are not available, we performed a protein structure homology modelling using the SWISS-MODEL automated server [45-48]. The template structure used was *Af*Nir (PDB 1SNR) which primary amino acid sequence shows about 84% of identity with wt *Sm*Nir. The high sequence identity, the full conserved residues coordinated to the copper centers, and the results of the test performed indicate that the structural model for *Sm*Nir and their variants has enough quality for the objective of the present study. The T2 copper atom was automatically added by the SWISS-MODEL server, while the T1 copper atom was added at the position corresponding to that of *Af*Nir.

The hydrogen atoms and the protonation states of the titratable residues (*e.g.* His, Glu, Asp) were added using the empirical PROPKA procedure using the pdb2pqr server at pH 7 [49]. The structure was solvated with water molecules within 30 Å around the metal centers using the VMD program with default parameters [50].

In order to neutralize the system, 22 Na^+ ions were added. A short molecular dynamics simulation was performed to relax the hydrogen atoms and the solvation water molecules by fixing the backbone atoms of all residues.

The combined quantum mechanics/molecular mechanics (QM/MM) calculations implemented in Gaussian 09 code [51] were performed to model various aspects of the structure of both wt *Sm*Nir and variants, such as stability, strength in binding of ligands, reorganization upon nitrite binding, the chemical path Cu-His-Cys-Cu *vs* Cu-Asp-Cys-Cu

and *vs* Cu-His-Asp-Cu, metal to ligand spin delocalization, and spin-spin interaction between copper atoms.

For the QM part two functionals were used, the spin-polarized WB97XD functional including empirical atom-atom dispersion corrections [52] and the B3LYP [53, 54], whereas for MM part the Amber classical force field was used [55]. The basis set for the atoms in the QM part was 6-31G(d).

We treated at the QM part the residues His342B, His136, and His171 (Asp171 for H171D), which ligand the copper atom at T2; His131, His181, Met186, and Cys172 (Asp172 for C172D), which ligand the copper atom at T1, and the second sphere residues Asp134, His291B, and Ile293B. In addition, five buried water molecules surrounding the T2 center were added based on the structure of *Af*Nir (PDB 1AS7) named accordingly with this structure as 1200-A, 578-B, 584-B, 619-B, and 1201-B. To model the resting state of the proteins a water molecule named 503-B coordinated to copper at T2-A was included in the QM part in both wild type and variant structures. $N^{\delta 1}$ and $N^{\varepsilon 2}$ of His291 were considered to be protonated while Asp134 was deprotonated, as suggested elsewhere [19, 56]. To study how wt *Sm*Nir and variants bind the nitrite molecule, a NO_2^- ion was coordinated to the T2 copper atom in a bidentate way through the O-atoms. The rest of the residues were treated at the MM level of theory. The structure of wt *Sm*Nir and both variants were optimized with the QM residues free to relax and keeping fixed in position the atoms treated with MM.

3. Results and Discussion

3.1. Molecular and spectroscopic properties of H172D and C171D

SDS-PAGE showed a unique band with molecular mass of ~ 42.5 kDa for both mutant proteins, (Figure S1), whereas gel filtration analysis indicated a trimeric structure, in line with *Sm*Nir [10]. This suggests that both point mutations do not affect the quaternary structure of *Sm*Nir.

Metal analysis identified 1.9(1) Cu/monomer for H171D, in agreement with the values expected for Nir having fully occupied T1 and T2 copper sites. In contrast to wt *Sm*Nir and H171D, C172D showed metal contents ranging from 0.7 to 1.3 Cu/monomer, lower than that expected for a protein that can potentially incorporate 2 Cu/monomer.

Fig. 2 shows the UV-vis absorption spectra of both protein variants together with that of wt *Sm*Nir at pH 6, the pH value where wt *Sm*Nir shows maximal enzyme activity [10]. The absorption spectrum of as-purified H171D (red line) shows absorption maxima at 466 nm (2.3 $mM^{-1}cm^{-1}$) and 579 nm (2.1 $mM^{-1}cm^{-1}$), similar to those of wt *Sm*Nir (black line, maxima at 456 nm, 3.3 $mM^{-1}cm^{-1}$, and at 586 nm, 2.9 $mM^{-1}cm^{-1}$). These bands are typical of green T1 copper sites [57], indicating that the mutation of His to Asp does not significantly modify the T1 site. The spectra showed no significant differences with pH in the 5-10 range (not shown) for both wild-type and H171D, which indicates that T1 is not affected by any acid-base equilibrium. The addition of sodium ascorbate or sodium dithionite led to the disappearance of all visible bands of H171D (not shown), as described for wt *Sm*Nir [10]. This indicates that the reduction potential of T1 is not significantly modified by the point mutation. As expected, the UV-vis spectrum of C172D did not show the typical T1 absorption bands, as the Cys ligand is essential to yield the typical spectroscopic features of T1 (Figure 2, blue spectrum).

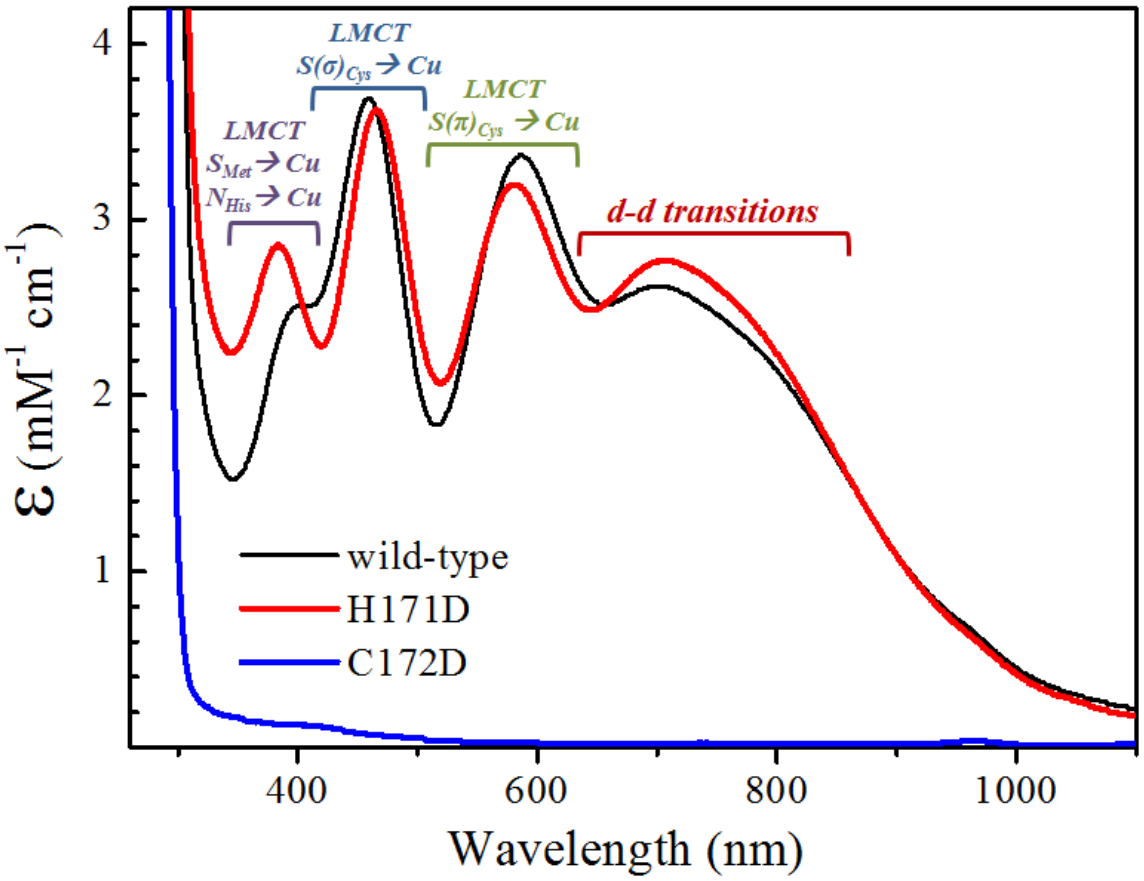

Fig. 2. UV-vis absorption spectra of wt *Sm*Nir, H171D, and C172D. The electronic transitions indicated on the figure are based on assignments reported elsewhere [58].

Representative EPR spectra of wt *Sm*Nir (upper), H171D (medium), and C172D (lower) obtained under different experimental conditions at pH 6.0 are shown in Fig. 3 (black solid lines) together with simulation (orange dotted lines). Experimental EPR spectra "a" and "b" correspond to as-purified and ascorbate reduced proteins, respectively. Simulation of as-purified wt *Sm*Nir EPR signal showed two overlapped spectral components associated with T1 (blue line, $g_{1,2,3}$=2.190, 2.052, 2.023; $A_{//}$= 7 mT) and T2 (red line, $g_{1,2,3}$= 2.315, 2.070, 2.065, $A_{//}$= 15 mT). Whereas the T1 center is completely reduced to the diamagnetic Cu^{+} oxidation state upon sodium ascorbate addition, only a small fraction (~ 10 %) of the T2 center remains as Cu^{2+} (spectrum b, upper panel). EPR analysis of as-purified H171D

(medium panel) yielded a good simulation assuming three overlapped nearly axial EPR signals, one corresponding to T1 ($g_{1,2,3}$=2.183, 2.052, 2.023; $A_{//}$=7.5 mT, blue), and other two T2 signals with different intensity ratio identified with roman numerals ($T2_I^{H171D}$: $g_{1,2,3}$=2.330, 2.075, 2.035, $A_{//}$=15 mT, red line; $T2_{II}^{H171D}$: $g_{1,2,3}$=2.280, 2.075, 2.030; $A_{//}$=17 mT, green line; $T1:T2_I:T2_{II}$ ratio of 1:0.35:0.65). $T1^{H171D}$ and $T2_{II}^{H171D}$ centers are reduced to the Cu^+ diamagnetic state upon addition of sodium ascorbate excess, whereas $T2_I^{H171D}$ partially remains in the oxidized form (spectrum b, medium panel). Addition of sodium dithionite excess under anaerobic conditions reduces completely the three copper species of H171D (not shown). The behavior towards sodium ascorbate and sodium dithionite of $T1^{H171D}$ and $T2_{II}^{H171D}$ is similar to that observed for both copper centers of wt *Sm*Nir (Fig. 3, upper panel A) and Nirs from other sources [20, 21, 23, 26, 32], in line with reduction potentials falling in the range of 300 mV to 0 mV *vs* SHE. In contrast, the reduction potential of $T2_I^{H171D}$ falls in the range of 0 mV to –400 mV, which is a value rather unusual for T2 centers of Nirs. Spin quantification of the EPR signal of as-purified H171D yielded ~ 2 spin/monomer, which indicates that T1 and both T2 species are completely oxidized under aerobic conditions.

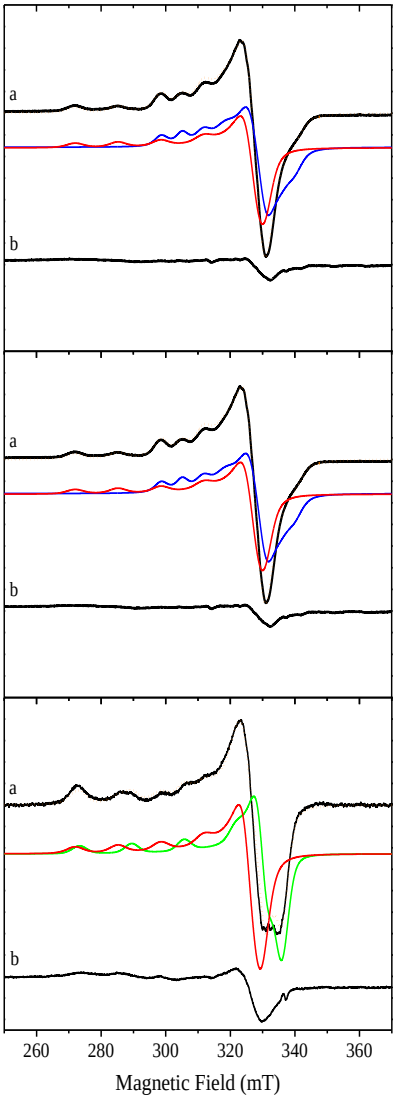

Fig. 3. EPR spectra (solid black lines) of wt *Sm*Nir (upper), H171D (medium), and C172D (lower) together with simulation. Simulations (orange dotted lines) are obtained by adding the individual components (colored solid lines). Spectra "a" in all panels correspond to as-purified protein whereas spectra "b" were obtained using an ascorbate/protein ratio of ~ 10:1. Spectral components associated with the different copper centers were identified by redox titrating the protein samples with increasing amounts of sodium ascorbate under anaerobic conditions.

As-purified C172D (lower panel) showed two type 2 Cu EPR spectral components in the same ratio, and, as expected, no T1 EPR signal. ($T2_I^{C172D}$= $g_{1,2,3}$=2.315, 2.075, 2.070, A_1= 15 mT, red line; $T2_{II}^{C172D}$: $g_{1,2=3}$=2.270, 2.045, A_1= 18 mT, green line). EPR features and redox behavior of $T2_I^{C172D}$ are very similar to that of T2 of as-purified wt *Sm*Nir,

suggesting that this center corresponds to the catalytically active copper site. In contrast, $T2_{II}^{C172D}$ is reduced to ~ half of the original intensity upon sodium ascorbate addition (spectrum b), indicating a more negative reduction potential than that of $T2_{I}^{C172D}$. The EPR features of $T2_{II}^{C172D}$, like those of $T2_{II}^{H171D}$, have no resemblance with any previous EPR signal reported in closely related enzymes. Spin quantification of T2 EPR signals of C172D yielded spin concentration of the order of the copper content, which indicates that copper ions of both $T2_{I}^{C172D}$ and $T2_{II}^{C172D}$ centers are completely oxidized in the as-purified protein. As said above, metal analysis of C172D yielded copper contents in the range of 0.7 to 1.3 Cu/monomer. This variability in copper content contrasts with that found in both wt *Sm*Nir and H171D (~ 2 Cu/monomer) and reflects the inability of C172D to incorporate a full metal content. Considering the inherent uncertainty in protein metal determination, the copper content of C172D suggests that copper is incorporated only at the level of the active site, in which case the two distinct EPR signals would indicate some T2 inhomogeneity. However, the facts that C172D shows essentially the same EPR signal in the range 0.7-1.3 Cu/monomer, *i.e.* EPR signals are independent of the protein metal content, and that there is not any structural reason at level of the active site justifying some inhomogeneity, suggest that copper ions associated with $T2_{II}^{C172D}$ could be incorporated at the original T1 site. These possibilities will be assessed by theoretical calculations below.

Since wt *Sm*Nir shows slight modifications in both $g_{//}$ and $A_{//}$ values upon nitrite-T2 interaction [10, 26, 32], we investigated the T2 EPR behavior of both protein variants upon sodium nitrite addition (Fig. S2). Both T2 EPR signals of H171D and that of $T2_{II}^{C172D}$ were not modified upon sodium nitrite addition, which suggests that these T2 sites do not behave like a typical T2 active site. In contrast, $T2_{I}^{C172D}$ shows a behavior similar to that observed for T2 of wt *Sm*Nir, indicating that this center could be catalytically competent.

3.2. Kinetic assays using MV and SmPaz as electron donors.

Steady state kinetic studies using the artificial electron donor MV indicated that H171D showed no detectable activity under the assay conditions, whereas C172D exhibited very low activity (k_{cat}= 3.9(4) s^{-1}) compared to that of wt *Sm*Nir (k_{cat}= 240(50) s^{-1}), showing that this protein variant retains some ability to catalyze nitrite to NO. The latter is in contrast with the mutation of Cys to Ala in *Af*Nir, which showed no activity using the same electron donors [29]. The low turnover number observed for C172D could be attributed to slow substrate binding rates (*i.e.* small k_{on} and/or large k_{off}), which is in line with the decrease in K_m value (K_m = 1.4(3) mM for C172D, K_m = 3.6(3) mM for wt *Sm*Nir, Fig. S3). Note that the K_m value reported here for wt *Sm*Nir is different to that reported previously [10], due to the different experimental conditions employed in the kinetic assay (see experimental section for details). This fact suggests that both MV oxidation and nitrite reduction might occur through a ping-pong mechanism occurring completely at the active site. Then, for steric reasons it is expected a substituted enzyme mechanism without accumulation of ternary complex, implying that nitrite should bind T2 in its Cu^+ state. There are some examples in the literature of Cu(I) and Cu(II) complexes which can reduce nitrite to NO [59, 60]. The reduction of nitrite in a Cu^+ site might explain the low turnover number observed in C172D relative to that of wt *Sm*Nir, since T2(Cu^+)-nitrite interaction is electrostatically less favorable than that for T2(Cu^{2+})-nitrite complex.

Kinetic studies with the physiological electron donor *Sm*Paz using steady state kinetics (Fig. S4A) and protein electrochemistry (Fig. S4B and S4C) showed no activity towards nitrite in both protein variants.

3.3. QM/MM studies of SmNir and its protein variants

QM/MM calculation was started from a homology model of a known structure of the green type *Af*Nir, as described in Computational Methods (section *2.6*). The resulting wt *Sm*Nir structure is presented in panel A of Fig. 4 compared with a recent crystal structure of wt *Af*Nir (PDB 5F7B), which showed a T2 site with the apical O atom assigned to a water molecule in two possible positions with 30 % and 70 % occupation (see Figure 4) [19]. As shown in this figure, both structural models are similar and show an r.m.s deviation of 0.2 Å for the atoms treated as QM. The water molecule 503B coordinated to T2 (d_{Cu-O}= 1.90 Å) ends in a position close to the water molecule with lower occupancy in the X-ray *Af*Nir structure (Fig. 4) [19]. This T2 water ligand is also hydrogen bonded to the closest Asp134, which forms part of the sensing loop (Fig. 1). In addition, the hydrogen bond between $N^{\delta 1}$ of His171 and the carbonyl O atom of Cys172 present in *Af*Nir was also obtained in our model. All the water molecules included in our model whose positions were crystallographycally determined showed no significant differences in atomic coordinates relative to those determined by X-ray data. We thus concluded that our QM/MM model of wt *Sm*Nir is robust enough to continue with the proposed goals. All QM/MM structures in PDB format are available upon request.

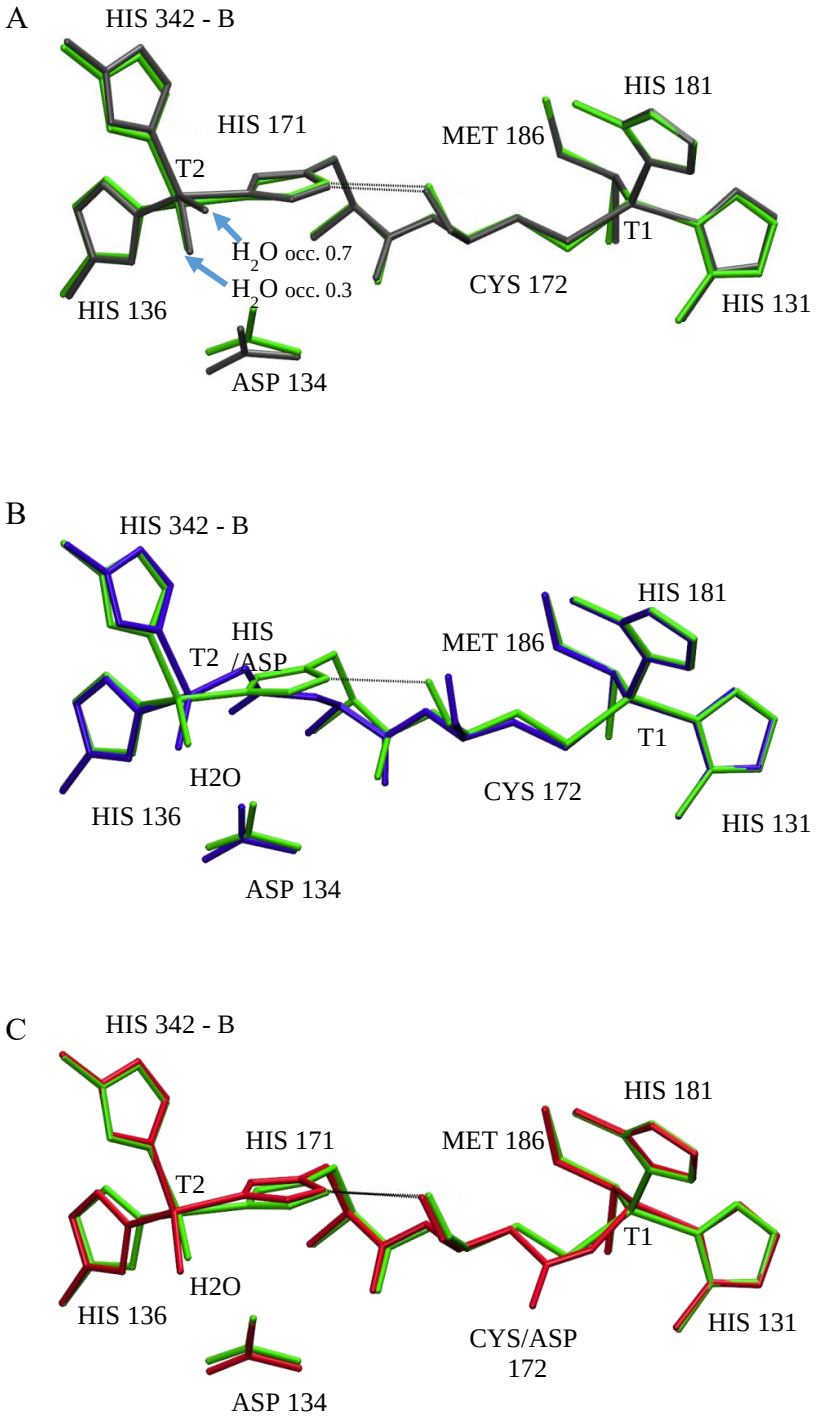

Fig. 4. A) Superposition of optimized QM/MM structure of wt *Sm*Nir (green) with the X-ray structure of wt *Af*Nir (gray, PDB 5F7B). B) Superposition of optimized QM/MM structures of H171D (blue) with that of wt *Sm*Nir. C) idem B but for C172D (red). The $N^{\delta 1}H\ldots O{=}C$ hydrogen bond is depicted as dotted lines. Only atoms treated by QM are

shown. Hydrogen atoms were removed for clarity. PDB files obtained by QM/MM for wt *Sm*Nir, H171D, and C172D can be obtained upon request.

Comparison of wt *Sm*Nir and H171D QM/MM structures is presented in panel B of Fig. 4. The T1-T2 distance reduced from 12.6 Å to 12.2 Å due to the slightly shorter length of Asp compared with His. The T1 site is similar in both structures, in line with the UV-vis and EPR results, while the T2 site of the protein variant shows the side chain carboxylate of Asp171 coordinated to the copper atom in an essentially monodentate fashion (d_{Cu-O} of 1.90 Å and 3.03 Å). All attempts to move the carboxylate group and to rotate the backbone yielded always the coordination mode showed in the fig., *i.e.* monodentate is the most stable structure as observed in solid state copper complexes with aspartic acid [61, 62]. These results suggest that the carboxylate binding mode is determined by competition with His342 and His136 at the T2 site and also with the T1 site residues. Similar to wt *Sm*Nir, H171D presents a water molecule coordinated to the T2 copper atom at 1.90 Å. This water molecule is stabilized through a strong hydrogen bond with Asp134 and a somewhat weaker bond with the bridging water 1200A, which is also hydrogen bonded to the second sphere ligand His291. This fact, together with that all water molecules treated at quantum level and non-exchanged amino acids maintained their positions respect to the wt structure, is indicating that the amino acid exchange does not affect the rest of the protein considered essential for catalysis, *e.g.* the sensing loop peptide bridge and the H-bonded water molecules network (QM/MM structures in pdb format are available upon request). The same conclusion was obtained for the C172D variant presented below. However, EPR spectral analysis showed two different type 2 copper sites, which reveals certain inhomogeneity in the structure of T2. This T2 inhomogeneity could be ascribed either to different positions of the T2 water ligand, as observed in the closely related *Af*Nir [19], and/or to a different coordination mode of the aspartic acid moiety (Asp171), as observed

in X-ray structural data of Mo-containing proteins in which aspartic acid side chain can adopt mono- or bidentate coordination modes [63]. Another remarkable structural feature is the absence of the $N^{\delta 1}H\ldots O{=}C$ hydrogen bond in the T1-T2 pathway proposed to be essential in the electron transfer of green Nirs [38]. Hence, the T1-T2 bridging pathway in this protein variant is rather different compared to that of wt *Sm*Nir, which could be a possible cause for the lack of catalytic activity of H171D.

To analyze whether the lack of activity of H171D is a problem of nitrite binding at T2 or to an inefficient T1-T2 electron transfer pathway, we performed QM/MM calculations on nitrite-bound forms of both wt *Sm*Nir and H171D (PDB files obtained are given as supplementary material). Calculations on the protein variant showed that, like in wt *Sm*Nir, nitrite coordinates to T2 in a bidentate fashion through the O atoms, as observed in the X-ray structure of nitrite soaked Nir crystals [64, 65], and also observed in several copper complexes [66-68]. Our calculations show a coordination mode forming an angle of 10° and 5° between ONO and OCuO planes for wt *Sm*Nir and H171D, respectively, in line with previous calculations [66], but slightly lower than the one obtained in some X-ray structures of Nir.[19, 64] The position of the nitrite anion is primarily stabilized by Asp134 and Ile293. Since the reaction mechanism of Nirs implies the oxygen ligand removal for nitrite binding, we evaluated the energetic cost of removing this ligand in both wt *Sm*Nir and H171D. This calculation showed that the relative energy to remove the T2 oxygenic ligand in both protein forms is similar (Fig. S5), implying that the lack of activity of H171D cannot be ascribed to a substrate-active site binding reason. These results altogether suggest that the lack of catalytic activity in this protein variant is due to an inefficient T1-T2 electron transfer pathway, more specifically to the absence of the proposed electron transfer pathway $N^{\delta 1}H\ldots O{=}C$ hydrogen bond.

Panel C of Fig. 4 compares QM/MM structure of C172D with that of wt *Sm*Nir assuming that the protein variant contains 2 copper atoms per monomer. Since C172D showed copper contents in the range of 0.7 to 1.3 Cu/monomer, which is not conclusive whether the original T1 site is metallated or not, calculations for this protein variant were also performed assuming that only the active site is metallated. A superposition of the C172D structures assuming 1 and 2 copper atoms per monomer is given as supplementary material (Fig. S6). T2 site in both structural models is similar to that of wt *Sm*Nir, showing only small differences in binding distances of the imidazole moieties. Also, the hydrogen bond proposed to be essential in the electron transfer is conserved in both cases. For the 2 Cu/monomer-containing C172D structural model, calculations showed a copper center at the original *Sm*Nir T1 site in a tetrahedral coordination as in wt *Sm*Nir in which the aspartic acid carboxylate side chain is bound in a monodentate fashion with Cu-O distances of 1.97 Å and 4.05 Å. The presence of two copper centers in this protein variant is in line with the two distinct T2 EPR-detected copper centers, which implies that the catalytically active $T2_I^{C172D}$ center should correspond to the active site, whereas $T2_{II}^{C172D}$ to the modified T1. Note that this possibility would imply the coexistence of four protein subpopulations: one where both available coordinating environments contain copper, another one without copper, and two others in which copper is present only at T2 or only at modified T1. However, as the copper content in the mutant protein yielded values around 1 copper atom per monomer, and that there are no observable d-d transitions associated with a Cu(II) ion at the modified T1 center (see Fig. 2), it cannot be excluded that only the active site is fully occupied, in which case the two EPR signals should correspond to some inhomogeneity in this copper center.

3.4. Nitrite reoxidation of reduced SmNir: Role of the $N^{\delta 1}H...O=C$ hydrogen bond in T1-T2 electron transfer

Catalytic activity of *Sm*Nir as well as those of other Nirs showed an important pH dependence with maximal activity around pH 5-6 and almost undetectable activity at pH > 9 [10, 22, 23, 69, 70]. This pH dependence has been suggested to be produced by different factors such as structural modifications of T2, mainly a rotation of the Cu-H_2O bond, T2-neighboring amino acids changes, and proton transfer from Asp 134 to nitrite bound T2 copper center, which triggers T1-T2 electron transfer [20, 23, 24, 71]. However, our results on H171D and C172D protein variants suggest that the $N^{\delta 1}H…O=C$ hydrogen bond of the Cys-His bridge may also play an important role in electron transfer between both copper centers.

To obtain experimental support on the latter possibility, we evaluated the EPR and UV-vis spectroscopic behavior of dithionite reduced *Sm*Nir at pH 6 and 10 upon nitrite addition (Fig. 5). In contrast to that observed at pH 6 (Fig. 3), *Sm*Nir at high pH showed two T2 type overlapping EPR signals with an intensity ratio of 0.65:0.35; a simulation of the EPR spectrum at pH 10 is given in Fig. S7. The signal with minor intensity ($g_{1,2,3}$= 2.231, 2.056, 2.038, A_1= 20.7 mT) likely corresponds to non-protein copper ion species produced during pH increase, assignment based on the fact that a solution of copper sulfate in the protein buffer showed the same signal. Hence, the more intense EPR component corresponds to the T2 center, but with a different structure to that at pH 6, as indicated by the different EPR parameters obtained by simulation ($g_{1,2,3}$= 2.345, 2.105, 2.045; A_1= 11.5 mT). The pH-dependent structural changes of T2 are reversible, as the T2 EPR signal at pH 6 is recovered upon pH cycling the enzyme. That the process is reversible was also confirmed

by kinetic assays that showed that the pH cycling of the enzyme recovered the enzyme catalytic activity.

Given that both structure and function are reversible on pH cycling, we evaluated the kinetic ability of *Sm*Nir at both pH using sodium dithionite as electron donor by adding an excess of nitrite relative to dithionite monitoring the oxidation state of each copper centers. Left panels of Fig. 5 show these experiments for the active enzyme at pH 6, in which reoxidation of both copper centers is shown by EPR whereas T1 reoxidation by UV-vis. These results confirm both nitrite/T2 interaction and T1-T2 ET pathway integrity at pH 6. A different situation is observed when the same experiment is conducted at pH 10 (right panels). The EPR spectrum **c** showed the partial recovery of the Cu^{2+}-T2 EPR signal, whereas the UV-vis spectrum **c** did not show the Cu^{2+}-T1 absorption bands upon nitrite addition. The former clearly indicates that the T2 center can react with nitrite at pH 10, in line with X-ray structural data of *Rs*Nir at high pH [23], whereas the absence of spectroscopic features associated with oxidized T1 indicates that the lack of activity at pH > 9 under the experimental conditions of the method is caused by a deficient T1-T2 electron transfer.

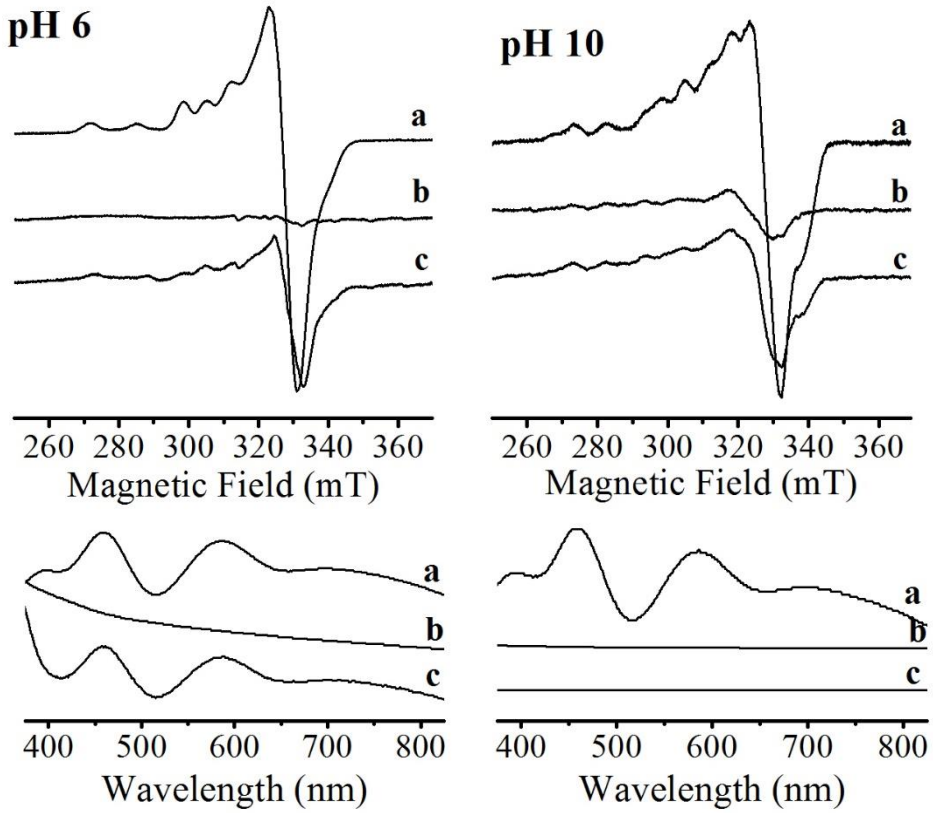

Fig. 5. Reoxidation experiments of dithionite reduced *Sm*Nir at pH 6 (left panels) and 10 (right panels) monitored by EPR (upper) and UV-vis (lower) spectroscopies upon sodium nitrite addition. Spectra a, as-purified *Sm*Nir; spectra b, dithionite reduced *Sm*Nir; spectra c, idem b but upon addition of nitrite excess (nitrite:dithionite ratio of 5:1).

As commented above, T1-T2 electron transfer rate with and without nitrite is pH dependent and presents a maximum around pH 6. Our present results show that the T2 site at high pH can reoxidize nitrite, and hence the loss of activity may be ascribed to an interruption of the T1-T2 electron transfer pathway. The T2 reoxidation implies that the two proton-coupled nitrite reduction can be carried out independently of the pH of the reaction mixture, whereas the absence of the T1 UV-vis features points to structural modifications of the Cys-His bridge. The unique pH-dependent molecular structure in this pathway is the $N^{\delta 1}H\ldots O{=}C$ hydrogen bond that shortcuts the T1-T2 covalent bridge (Fig. 1 and 4), which

is suggesting that at high pH this hydrogen bond can be broken by proton transfer to either an acceptor group (e.g. a neighboring carbonyl group) or to a solvent molecule. This assumption is based on theoretical studies of Zn-containing proteins and model systems that showed that the metal-coordinated histidine imidazole moiety may be deprotonated in those cases of solvent exposed metal centers with strong Lewis acid character, which in addition must have neighboring proton acceptors in the histidine imidazole vicinity [72].

Both T1 and T2 centers in as-purified Nirs constitute a paramagnetic binuclear system of two *S*=1/2 spins. Determining the isotropic exchange interaction that couples both spins is important as its value is directly related to the electron transfer rate between T1 and T2 when the exchange and electron transfer pathways are the same [73]. Our experimental and theoretical results show that the presence of the $N^{\delta 1}H\ldots O{=}C$ hydrogen bond that shortcuts the T1-T2 covalent bridge is essential in T1-T2 electron transfer process, which means that evaluating the T1-T2 exchange interaction associated with this chemical pathway could be useful to give some insight in the Nir reaction mechanism. Previous theoretical studies of Nirs evaluated that the copper centers are coupled by isotropic exchange with $2J$= -0.066 cm^{-1} (H_{ex}= $-2J\ \mathbf{S}_1.\mathbf{S}_2$) [38]. Consequently, we performed computational calculations to evaluate the exchange interaction in *Sm*Nir and its variants using a method we reported previously for bioinorganic model systems [74]. Our computational results regarding the magnitude of T1-T2 exchange interaction are not conclusive, since the calculated *J*-values fell within the error limit of the method (~ 0.01 cm^{-1}). This is in line with EPR experimental results that did not detect measurable exchange interaction between copper centers (The *J*-value lower limit detected by X-band CW EPR is of the order of ~ 0.001 cm^{-1}). That no *J*-value was detected could be a matter of controversy. One can wonder whether this rather weak hydrogen bond ($d_{D\text{-}A}$ ~ 2.8 Å) plays an essential role in T1-T2 electron transfer or not.

Our experimental kinetic results indicate that this might be the case. We have recently reported that very weak hydrogen bonds with d_{D-A} distances > 2.8 Å like that of Nirs can transmit non-negligible exchange interactions ($0.02 < J < 0.8$ cm^{-1}). The fact that in this work isotropic exchange interaction could be neither theoretically calculated nor experimentally measured is evidently associated with the long linear T1-T2 distance (~ 12 Å).

4. Conclusion

The two mononuclear copper centers of *Sm*Nir are bridged by a Cys-His chemical pathway which acts as electron transfer conduit for nitrite reduction. This chemical pathway involves two subpathways: a pure covalent one formed by the protein backbone and the Cys and His side chains, and a second one that includes the $N^{\delta 1}H\ldots O{=}C$ hydrogen bond that partially shortcuts the covalent pathway. Mutation of the histidine moiety to aspartic acid yielded a protein variant containing T1 and T2 centers bridged by a single covalent pathway which does not show the hydrogen bond named above. This variant retains the ability to bind nitrite but is catalytically incompetent with both artificial and physiological electron donors, which suggests the relevance of the hydrogen bond in T1-T2 electron transfer. Mutation of cysteine to aspartic acid yielded a protein variant with two type 2 copper centers with one of them being identical to the wt *Sm*Nir T2 active site. C172D is, like H171D, inactive towards nitrite with the physiological electron donor, but active using artificial electron donors. This confirms that nitrite reduction can occur entirely at T2 through a substituted enzyme mechanism without accumulation of ternary complex.

Investigating the catalytic activity of *Sm*Nir as a function of pH showed that the enzyme presents maximal activity around pH 5-6 and almost undetectable activity at pH > 9 and

that its structure and function are completely reversible upon pH cycling. Reoxidation experiments showed that at high pH the T2 site can produce the two-proton coupled reduction of nitrite in a T1-decoupled way, as observed for the C172D variant. This fact confirms that the loss of activity at high pH is due to reversible structural modifications of the T1-T2 electron transfer pathway. Previous studies hypothesized that the pH-dependent catalytic activity originates from structural modifications of both T2 and T2-neighboring amino acids which would preclude T1-T2 electron transfer. In contrast, our studies on *Sm*Nir point to the rupture of the $N^{\delta 1}H\ldots O{=}C$ hydrogen bond in the Cys-His bridge as the possible cause. Despite the electronic structures of T1centers in blue and green type Nir being different, the $N^{\delta 1}H\ldots O{=}C$ hydrogen bond is present in both types of enzymes, which suggests that T1-T2 electron transfer should be conducted through this hydrogen bond in both type of enzymes. However, whether present results in a green type Nir can be extrapolated to blue type ones or not requires of additional experimental work.

Acknowledgments

We thank FONCyT, CONICET, and CAI+D-UNL for financial support. M.G.R., P.J.G, S.D.D., F.M.F. and C.D.B are members of CONICET (Argentina). J.C.C. and M.C.G. thank CONICET for fellowship grants.

References

[1] W.G. Zumft, Cell biology and molecular basis of denitrification, Microbiol. Mol. Biol. Rev., 61 (1997) 533-616.
[2] B.A. Averill, Dissimilatory Nitrite and Nitric Oxide Reductases, Chem. Rev., 96 (1996) 2951-2964.
[3] M.J. Barnett, R.F. Fisher, T. Jones, C. Komp, A.P. Abola, F. Barloy-Hubler, L. Bowser, D. Capela, F. Galibert, J. Gouzy, M. Gurjal, A. Hong, L. Huizar, R.W. Hyman, D. Kahn, M.L. Kahn, S. Kalman, D.H. Keating, C. Palm, M.C. Peck, R. Surzycki, D.H. Wells, K.C. Yeh, R.W. Davis, N.A. Federspiel, S.R. Long, Nucleotide sequence and predicted functions of the entire Sinorhizobium meliloti pSymA megaplasmid, Proc. Natl. Acad. Sci. U.S.A., 98 (2001) 9883-9888.
[4] J.W. Godden, S. Turley, D.C. Teller, E.T. Adman, M.Y. Liu, W.J. Payne, J. LeGall, The 2.3 angstrom X-ray structure of nitrite reductase from Achromobacter cycloclastes, Science, 253 (1991) 438-442.
[5] M. Kukimoto, M. Nishiyama, M.E.P. Murphy, S. Turley, E.T. Adman, S. Horinouchi, T. Beppu, X-ray Structure and Site-Directed Mutagenesis of a Nitrite Reductase from Alcaligenes Faecalis S-6: Roles of Two Copper Atoms in Nitrite Reduction, Biochemistry, 33 (1994) 5246-5252.
[6] T. Inoue, M. Gotowda, Deligeer, K. Kataoka, K. Yamaguchi, S. Suzuki, H. Watanabe, M. Gohow, Y. Kai, Type 1 Cu structure of blue nitrite reductase from Alcaligenes xylosoxidans GIFU 1051 at 2.05 Å resolution: Comparison of blue and green nitrite reductases, J. Biochem., 124 (1998) 876-879.
[7] Y. Fukuda, H. Koteishi, R. Yoneda, T. Tamada, H. Takami, T. Inoue, M. Nojiri, Structural and functional characterization of the Geobacillus copper nitrite reductase: involvement of the unique N-terminal region in the interprotein electron transfer with its redox partner, Biochimica et biophysica acta, 1837 (2014) 396-405.
[8] T.J. Lawton, K.E. Bowen, L.A. Sayavedra-Soto, D.J. Arp, A.C. Rosenzweig, Characterization of a Nitrite Reductase Involved in Nitrifier Denitrification, J. Biol. Chem., 288 (2013) 25575-25583.
[9] M.J. Boulanger, M.E.P. Murphy, Crystal structure of the soluble domain of the major anaerobically induced outer membrane protein (AniA) from pathogenic Neisseria: a new class of copper-containing nitrite reductases1, J. Mol. Biol., 315 (2002) 1111-1127.
[10] F.M. Ferroni, S.A. Guerrero, A.C. Rizzi, C.D. Brondino, Overexpression, purification, and biochemical and spectroscopic characterization of copper-containing nitrite reductase from Sinorhizobium meliloti 2011. Study of the interaction of the catalytic copper center with nitrite and NO, J. Inorg. Biochem., 114 (2012) 8-14.
[11] F.E. Dodd, J. Van Beeumen, R.R. Eady, S.S. Hasnain, X-ray structure of a blue-copper nitrite reductase in two crystal forms. The nature of the copper sites, mode of substrate binding and recognition by redox partner, J. Mol. Biol., 282 (1998) 369-382.
[12] E. Libby, B.A. Averill, Evidence that the Type 2 copper centers are the site of nitrite reduction by Achromobacter cycloclastes nitrite reductase, Biochem. Biophys. Res. Commun., 187 (1992) 1529-1535.
[13] S. Suzuki, K. Kataoka, K. Yamaguchi, T. Inoue, Y. Kai, Structure–function relationships of copper-containing nitrite reductases, Coord. Chem. Rev. , 190–192 (1999) 245-265.

[14] L.M. Murphy, F.E. Dodd, F.K. Yousafzai, R.R. Eady, S.S. Hasnain, Electron donation between copper containing nitrite reductases and cupredoxins: the nature of protein-protein interaction in complex formation1, J. Mol. Biol., 315 (2002) 859-871.
[15] R.W. Strange, L.M. Murphy, F.E. Dodd, Z.H.L. Abraham, R.R. Eady, B.E. Smith, S.S. Hasnain, Structural and kinetic evidence for an ordered mechanism of copper nitrite reductase1, J. Mol. Biol. , 287 (1999) 1001-1009.
[16] M.J. Boulanger, M. Kukimoto, M. Nishiyama, S. Horinouchi, M.E.P. Murphy, Catalytic Roles for Two Water Bridged Residues (Asp-98 and His-255) in the Active Site of Copper-containing Nitrite Reductase, J. Biol. Chem., 275 (2000) 23957-23964.
[17] K. Kataoka, H. Furusawa, K. Takagi, K. Yamaguchi, S. Suzuki, Functional Analysis of Conserved Aspartate and Histidine Residues Located Around the Type 2 Copper Site of Copper-Containing Nitri Reductase1, J. Biochem., 127 (2000) 345-350.
[18] S. Suzuki, T. Kohzuma, Deligeer, K. Yamaguchi, N. Nakamura, S. Shidara, K. Kobayashi, S. Tagawa, Pulse Radiolysis Studies on Nitrite Reductase from Achromobacter cycloclastes IAM 1013: Evidence for Intramolecular Electron Transfer from Type 1 Cu to Type 2 Cu, J. Am. Chem. Soc., 116 (1994) 11145-11146.
[19] Y. Fukuda, K.M. Tse, T. Nakane, T. Nakatsu, M. Suzuki, M. Sugahara, S. Inoue, T. Masuda, F. Yumoto, N. Matsugaki, E. Nango, K. Tono, Y. Joti, T. Kameshima, C. Song, T. Hatsui, M. Yabashi, O. Nureki, M.E.P. Murphy, T. Inoue, S. Iwata, E. Mizohata, Redox-coupled proton transfer mechanism in nitrite reductase revealed by femtosecond crystallography, Proc. Natl. Acad. Sci. U.S.A., 113 (2016) 2928-2933.
[20] N.G.H. Leferink, C. Han, S.V. Antonyuk, D.J. Heyes, S.E.J. Rigby, M.A. Hough, R.R. Eady, N.S. Scrutton, S.S. Hasnain, Proton-coupled electron transfer in the catalytic cycle of Alcaligenes xylosoxidans copper-dependent nitrite reductase, Biochemistry, 50 (2011) 4121-4131.
[21] F. Ferroni, J. Marangon, N. Neuman, J. Cristaldi, S. Brambilla, S. Guerrero, M. Rivas, A. Rizzi, C. Brondino, Pseudoazurin from Sinorhizobium meliloti as an electron donor to copper-containing nitrite reductase: influence of the redox partner on the reduction potentials of the enzyme copper centers, J. Biol. Inorg. Chem., 19 (2014) 913-921.
[22] Z.H. Abraham, B.E. Smith, B.D. Howes, D.J. Lowe, R.R. Eady, pH-dependence for binding a single nitrite ion to each type-2 copper centre in the copper-containing nitrite reductase of Alcaligenes xylosoxidans, Biochem. J, 324 (1997) 511-516.
[23] F. Jacobson, A. Pistorius, D. Farkas, W. De Grip, Ã.r. Hansson, L. SjÃ¶lin, R. Neutze, pH Dependence of Copper Geometry, Reduction Potential, and Nitrite Affinity in Nitrite Reductase, J. Biol. Chem., 282 (2007) 6347-6355.
[24] K. Kobayashi, S. Tagawa, Deligeer, S. Suzuki, The pH-dependent changes of intramolecular electron transfer on copper-containing nitrite reductase, J. Biochem., 126 (1999) 408-412.
[25] A. Veselov, K. Olesen, A. Sienkiewicz, J.P. Shapleigh, C.P. Scholes, Electronic Structural Information from Q-Band ENDOR on the Type 1 and Type 2 Copper Liganding Environment in Wild-Type and Mutant Forms of Copper-Containing Nitrite Reductase, Biochemistry, 37 (1998) 6095-6105.
[26] D. Pinho, S. Besson, C.D. Brondino, B. de Castro, I. Moura, Copper-containing nitrite reductase from Pseudomonas chlororaphis DSM 50135, Eur. J. Biochem., 271 (2004) 2361-2369.
[27] M. Prudêncio, R.R. Eady, G. Sawers, Catalytic and spectroscopic analysis of blue copper-containing nitrite reductase mutants altered in the environment of the type 2 copper centre: Implications for substrate interaction, Biochem. J., 353 (2001) 259-266.

[28] M.J. Ellis, S.V. Antonyuk, R.W. Strange, G. Sawers, R.R. Eady, S.S. Hasnain, Observation of an unprecedented Cu bis-his site: Crystal structure of the H129V mutant of nitrite reductase, Inorg. Chem., 43 (2004) 7591-7593.
[29] M.A. Hough, M.J. Ellis, S. Antonyuk, R.W. Strange, G. Sawers, R.R. Eady, S.S. Hasnain, High resolution structural studies of mutants provide insights into catalysis and electron transfer processes in copper nitrite reductase, J. Mol. Biol., 350 (2005) 300-309.
[30] M.E.P. Murphy, S. Turley, M. Kukimoto, M. Nishiyama, S. Horinouchi, H. Sasaki, M. Tanokura, E.T. Adman, Structure of Alcaligenes faecalis Nitrite Reductase and a Copper Site Mutant, M150E, That Contains Zinc, Biochemistry, 34 (1995) 12107-12117.
[31] K. Kataoka, K. Yamaguchi, S. Sakai, K. Takagi, S. Suzuki, Characterization and function of Met150Gln mutant of copper-containing nitrite reductase from Achromobacter cycloclastes IAM1013, Biochem. Biophys. Res. Commun., 303 (2003) 519-524.
[32] K. Olesen, A. Veselov, Y. Zhao, Y. Wang, B. Danner, C.P. Scholes, J.P. Shapleigh, Spectroscopic, Kinetic, and Electrochemical Characterization of Heterologously Expressed Wild-Type and Mutant Forms of Copper-Containing Nitrite Reductase from Rhodobacter sphaeroides 2.4.3†, Biochemistry, 37 (1998) 6086-6094.
[33] O. Farver, R.R. Eady, G. Sawers, M. Prudêncio, I. Pecht, Met144Ala mutation of the copper-containing nitrite reductase from Alcaligenes xylosoxidans reverses the intramolecular electron transfer, FEBS Lett., 561 (2004) 173-176.
[34] L. Basumallick, R.K. Szilagyi, Y. Zhao, J.P. Shapleigh, C.P. Scholes, E.I. Solomon, Spectroscopic Studies of the Met182Thr Mutant of Nitrite Reductase: Role of the Axial Ligand in the Geometric and Electronic Structure of Blue and Green Copper Sites, J. Am. Chem. Soc., 125 (2003) 14784-14792.
[35] M.A. Hough, S.V. Antonyuk, R.W. Strange, R.R. Eady, S.S. Hasnain, Crystallography with Online Optical and X-ray Absorption Spectroscopies Demonstrates an Ordered Mechanism in Copper Nitrite Reductase, J. Mol. Biol., 378 (2008) 353-361.
[36] M. Prudêncio, G. Sawers, S.A. Fairhurst, F.K. Yousafzai, R.R. Eady, Alcaligenes xylosoxidans dissimilatory nitrite reductase: Alanine substitution of the surface-exposed histidine 139 ligand of the type 1 copper center prevents electron transfer to the catalytic center, Biochemistry, 41 (2002) 3430-3438.
[37] H.J. Wijma, M.J. Boulanger, A. Molon, M. Fittipaldi, M. Huber, M.E.P. Murphy, M.P. Verbeet, G.W. Canters, Reconstitution of the Type-1 Active Site of the H145G/A Variants of Nitrite Reductase by Ligand Insertion, Biochemistry, 42 (2003) 4075-4083.
[38] R.G. Hadt, S.I. Gorelsky, E.I. Solomon, Anisotropic Covalency Contributions to Superexchange Pathways in Type One Copper Active Sites, J. Am. Chem. Soc., 136 (2014) 15034-15045.
[39] F. Sanger, S. Nicklen, A.R. Coulson, DNA sequencing with chain-terminating inhibitors, Proc. Natl. Acad. Sci., 74 (1977) 5463-5467.
[40] O.H. Lowry, N.J. Rosebrough, A.L. Farr, R.J. Randall, Protein measurement with the Folin phenol reagent, J. Biol. Chem., 193 (1951) 265-275.
[41] U.K. Laemmli, Cleavage of structural proteins during the assembly of the head of bacteriophage T4, Nature, 227 (1970) 680-685.
[42] S. Ida, Purification to homogeneity of spinach nitrite reductase by ferredoxin-sepharose affinity chromatography, J. Biochem., 82 (1977) 915-918.
[43] F.M. Ferroni, M.G. Rivas, A.C. Rizzi, M.E. Lucca, N.I. Perotti, C.D. Brondino, Nitrate reduction associated with respiration in Sinorhizobium meliloti 2011 is performed by a membrane-bound molybdoenzyme, BioMetals, 24 (2011) 891-902.

[44] S. Stoll, A. Schweiger, EasySpin, a comprehensive software package for spectral simulation and analysis in EPR, J. Magn. Reson., 178 (2006) 42-55.
[45] M. Biasini, S. Bienert, A. Waterhouse, K. Arnold, G. Studer, T. Schmidt, F. Kiefer, T.G. Cassarino, M. Bertoni, L. Bordoli, T. Schwede, SWISS-MODEL: modelling protein tertiary and quaternary structure using evolutionary information, Nucleic Acids Res., 42 (2014) W252-W258.
[46] F. Kiefer, K. Arnold, M. Kunzli, L. Bordoli, T. Schwede, The SWISS-MODEL Repository and associated resources, Nucleic Acids Res., 37 (2009) D387-392.
[47] K. Arnold, L. Bordoli, J. Kopp, T. Schwede, The SWISS-MODEL workspace: a web-based environment for protein structure homology modelling, Bioinformatics, 22 (2006) 195-201.
[48] N. Guex, M.C. Peitsch, T. Schwede, Automated comparative protein structure modeling with SWISS-MODEL and Swiss-PdbViewer: a historical perspective, Electrophoresis, 30 Suppl 1 (2009) S162-173.
[49] T.J. Dolinsky, J.E. Nielsen, J.A. McCammon, N.A. Baker, PDB2PQR: an automated pipeline for the setup of Poisson-Boltzmann electrostatics calculations, Nucleic Acids Res., 32 (2004) W665-667.
[50] W. Humphrey, A. Dalke, K. Schulten, VMD: Visual molecular dynamics, J. Mol. Graph., 14 (1996) 33-38.
[51] M.J. Frisch, G.W. Trucks, H.B. Schlegel, G.E. Scuseria, M.A. Robb, J.R. Cheeseman, G. Scalmani, V. Barone, B. Mennucci, G.A. Petersson, H. Nakatsuji, M. Caricato, X. Li, H.P. Hratchian, A.F. Izmaylov, J. Bloino, G. Zheng, J.L. Sonnenberg, M. Hada, M. Ehara, K. Toyota, R. Fukuda, J. Hasegawa, M. Ishida, T. Nakajima, Y. Honda, O. Kitao, H. Nakai, T. Vreven, J. Montgomery, J. A., J.E. Peralta, F. Ogliaro, M. Bearpark, J.J. Heyd, E. Brothers, K.N. Kudin, V.N. Staroverov, R. Kobayashi, J. Normand, K. Raghavachari, A. Rendell, J.C. Burant, S.S. Iyengar, J. Tomasi, M. Cossi, N. Rega, J.M. Millam, M. Klene, J.E. Knox, J.B. Cross, V. Bakken, C. Adamo, J. Jaramillo, R. Gomperts, R.E. Stratmann, O. Yazyev, A.J. Austin, R. Cammi, C. Pomelli, J.W. Ochterski, R.L. Martin, K. Morokuma, V.G. Zakrzewski, G.A. Voth, P. Salvador, J.J. Dannenberg, S. Dapprich, A.D. Daniels, O. Farkas, J.B. Foresman, J.V. Ortiz, J. Cioslowski, D.J. Fox, Gaussian 09, Revision C.1. Gaussian, Inc., Wallingford CT, (2009).
[52] J.-D. Chai, M. Head-Gordon, Long-range corrected hybrid density functionals with damped atom-atom dispersion corrections, Phys. Chem. Chem. Phys., 10 (2008) 6615-6620.
[53] A.D. Becke, Density- functional thermochemistry. III. The role of exact exchange, J. Chem. Phys., 98 (1993) 5648-5652.
[54] C. Lee, W. Yang, R.G. Parr, Development of the Colle-Salvetti correlation-energy formula into a functional of the electron density, Phys. Rev. B, 37 (1988) 785-789.
[55] W.D. Cornell, P. Cieplak, C.I. Bayly, I.R. Gould, K.M. Merz, D.M. Ferguson, D.C. Spellmeyer, T. Fox, J.W. Caldwell, P.A. Kollman, A Second Generation Force Field for the Simulation of Proteins, Nucleic Acids, and Organic Molecules, J. Am. Chem. Soc., 117 (1995) 5179-5197.
[56] H. Zhang, M.J. Boulanger, A.G. Mauk, M.E.P. Murphy, Carbon Monoxide Binding to Copper-Containing Nitrite Reductase from Alcaligenes faecalis, J. Phys. Chem. B 104 (2000) 10738-10742.
[57] E.I. Solomon, R.K. Szilagyi, S. DeBeer George, L. Basumallick, Electronic Structures of Metal Sites in Proteins and Models: Contributions to Function in Blue Copper Proteins, Chem. Rev., 104 (2004) 419-458.

[58] E.I. Solomon, R.G. Hadt, Recent advances in understanding blue copper proteins, Coord. Chem. Rev. , 255 (2011) 774-789.
[59] W.-J. Chuang, I.J. Lin, H.-Y. Chen, Y.-L. Chang, S.C.N. Hsu, Characterization of A New Copper(I)−Nitrito Complex That Evolves Nitric Oxide, Inorg. Chem., 49 (2010) 5377-5384.
[60] R.C. Maji, S.K. Barman, S. Roy, S.K. Chatterjee, F.L. Bowles, M.M. Olmstead, A.K. Patra, Copper Complexes Relevant to the Catalytic Cycle of Copper Nitrite Reductase: Electrochemical Detection of NO(g) Evolution and Flipping of NO2 Binding Mode upon CuII → CuI Reduction, Inorg. Chem., 52 (2013) 11084-11095.
[61] R.F. Baggio, R. Calvo, C. Brondino, M.T. Garland, A.M. Atria, E. Spodine, A Novel Structure of (l-Aspartato)(1,10-phenanthroline)copper(II) Hydrate, Acta Crystallogr. Sect. C: Cryst. Struct. Commun., 51 (1995) 382-385.
[62] L. Antolini, G. Marcotrigiano, L. Menabue, G.C. Pellacani, Coordination behavior of L-aspartic acid: thermal, spectroscopic, magnetic, and structural properties of aqua(L-aspartato)(2,2'-bipyridine)copper(II) trihydrate, Inorg. Chem., 22 (1983) 141-145.
[63] P.J. Gonzalez, M.G. Rivas, C.S. Mota, C.D. Brondino, I. Moura, J.J.G. Moura, Periplasmic nitrate reductases and formate dehydrogenases: Biological control of the chemical properties of Mo and W for fine tuning of reactivity, substrate specificity and metabolic role, Coord. Chem. Rev., 257 (2013) 315-331.
[64] E.I. Tocheva, F.I. Rosell, A.G. Mauk, M.E.P. Murphy, Side-On Copper-Nitrosyl Coordination by Nitrite Reductase, Science, 304 (2004) 867-870.
[65] S.V. Antonyuk, R.W. Strange, G. Sawers, R.R. Eady, S.S. Hasnain, Atomic resolution structures of resting-state, substrate- and product-complexed Cu-nitrite reductase provide insight into catalytic mechanism, Proc. Natl. Acad. Sci. U.S.A., 102 (2005) 12041-12046.
[66] N. Lehnert, U. Cornelissen, F. Neese, T. Ono, Y. Noguchi, K.-i. Okamoto, K. Fujisawa, Synthesis and Spectroscopic Characterization of Copper(II)−Nitrito Complexes with Hydrotris(pyrazolyl)borate and Related Coligands, Inorg. Chem., 46 (2007) 3916-3933.
[67] H. Yokoyama, K. Yamaguchi, M. Sugimoto, S. Suzuki, CuI and CuII Complexes Containing Nitrite and Tridentate Aromatic Amine Ligand as Models for the Substrate-Binding Type-2 Cu Site of Nitrite Reductase, Eur. J. Inorg. Chem. , 2005 (2005) 1435-1441.
[68] C.E. Ruggiero, S.M. Carrier, W.B. Tolman, Reductive Disproportionation of NO Mediated by Copper Complexes: Modeling N2O Generation by Copper Proteins and Heterogeneous Catalysts, Angew. Chem. Int. Ed. , 33 (1994) 895-897.
[69] T. Kakutani, H. Watanabe, K. Arima, T. Beppu, A blue protein as an inactivating factor for nitrite reductase from Alcaligenes faecalis strain S-6, J. Biochem., 89 (1981) 463-472.
[70] S. Suzuki, K. Kataoka, K. Yamaguchi, Metal coordination and mechanism of multicopper nitrite reductase, Accounts of chemical research, 33 (2000) 728-735.
[71] S. Ghosh, A. Dey, Y. Sun, C.P. Scholes, E.I. Solomon, Spectroscopic and Computational Studies of Nitrite Reductase: Proton Induced Electron Transfer and Backbonding Contributions to Reactivity, J. Am. Chem. Soc., 131 (2009) 277-288.
[72] Lin, C. Lim, Factors Governing the Protonation State of Zn-Bound Histidine in Proteins: A DFT/CDM Study, J. Am. Chem. Soc., 126 (2004) 2602-2612.
[73] R. Calvo, R.A. Isaacson, M.L. Paddock, E.C. Abresch, M.Y. Okamura, A.L. Maniero, L.C. Brunel, G. Feher, EPR study of the semiquinone biradical QȦ-QḂ- in photosynthetic

reaction centers of Rhodobacter sphaeroides at 326 GHz: Determination of the exchange interaction Jo, J. Phys. Chem. B., 105 (2001) 4053-4057.
[74] A.L. Pérez, N.I. Neuman, R. Baggio, C.A. Ramos, S.D. Dalosto, A.C. Rizzi, C.D. Brondino, Exchange interaction between S = 1/2 centers bridged by multiple noncovalent interactions: Contribution of the individual chemical pathways to the magnetic coupling, Polyhedron, 123 (2017) 404-410.

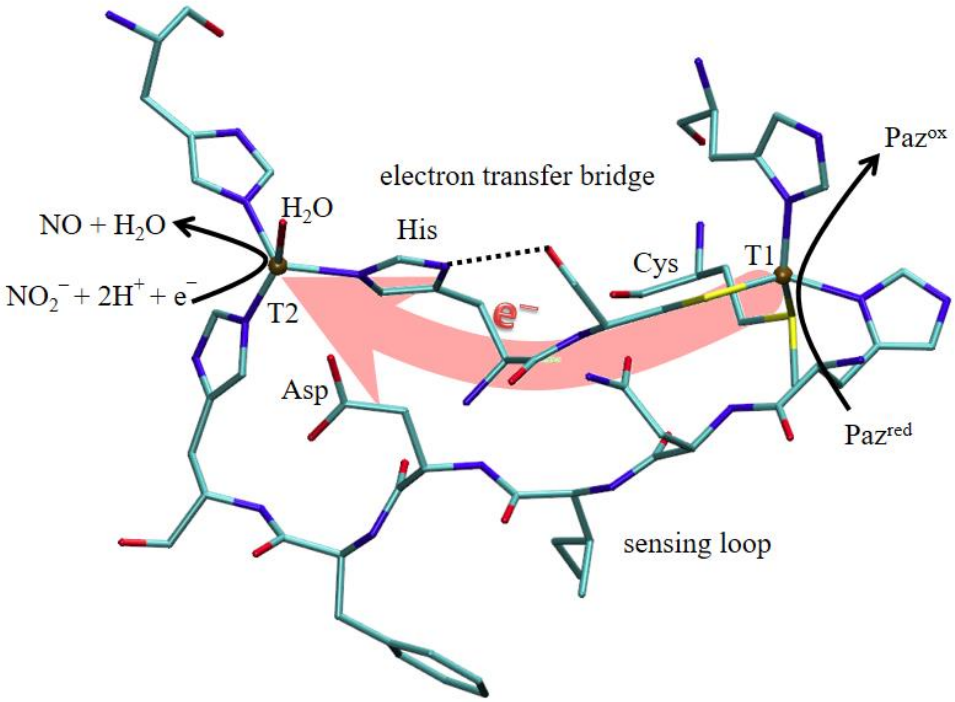

Graphical abstract

Highligths

- Cys-His bridge electron transfer pathway in a copper-containing nitrite reductase
- Site-directed mutagenesis, spectroscopic, and computational methods.
- Protein variants are catalytically incompetent towards physiological electron donor
- Changes in the Cys-His bridge interrupts the T1-T2 electron transfer
- The $N^{\delta 1}H\ldots O{=}C$ hydrogen bond is essential for catalysis